Supplementary information for

Patterns and drivers of soil microbial carbon use efficiency across soil depths in forest ecosystems

Junmin Pei[1,2], Jinquan Li[1], Yiqi Luo[3], Matthias C. Rillig[4,5], Pete Smith[6], Wenjing Gao[1], Bo Li[1,7], Changming Fang[1], Ming Nie[1]

Affiliations:

[1] State Key Laboratory of Wetland Conservation and Restoration, National Observations and Research Station for Wetland Ecosystems of the Yangtze Estuary, Ministry of Education Key Laboratory for Biodiversity Science and Ecological Engineering, and Institute of Eco-Chongming, School of Life Sciences, Fudan University, Shanghai, China.

[2] College of Life Sciences, Shanghai Normal University, Shanghai, China.

[3] School of Integrative Plant Science, Cornell University, Ithaca, NY, USA.

[4] Institute of Biology, Freie Universität Berlin, Berlin, Germany.

[5] Berlin-Brandenburg Institute of Advanced Biodiversity Research (BBIB), Berlin, Germany.

[6] Institute of Biological and Environmental Sciences, School of Biological Sciences, University of Aberdeen, Aberdeen, UK.

[7] State Key Laboratory for Vegetation Structure, Functions and Construction, Ministry of Education Key Laboratory for Transboundary Ecosecurity of Southwest China, Institute of Biodiversity, School of Ecology and Environmental Science and Southwest United Graduate School, Yunnan University, Kunming, China.

Contents of this file

Supplementary Text

Microbial diversity was characterized using high-throughput amplicon sequencing. Total genomic DNA was extracted from soil samples using the PowerSoil DNA Kit (Qiagen, Carlsbad, USA) following the manufacturer's instructions. Fungal communities were profiled by amplifying the internal transcribed spacer 2 (ITS2) region of the nuclear ribosomal DNA using primers described by Tedersoo et al.[1], with a unique sample-specific barcode incorporated upstream of the reverse primer[2]. Bacterial communities were assessed by targeting the V4 region of the 16S rRNA gene using the primer pair 515F (5′-GTGYCAGCMGCCGCGGTAA-3′) and 806R (5′-GGACTACNVGGGTWTCTAAT-3′)[3,4]. A 12-bp barcode and a 2-bp linker sequence (5′-TC-3′) were added between the barcode and the forward primer (5′-NNNNNNNNNNNNTC-515F-3′) to uniquely index each PCR product. Amplicons were stored at −20 °C prior to downstream processing, quantified using the Qubit dsDNA High Sensitivity Assay Kit (Invitrogen, Darmstadt, Germany), pooled in equimolar concentrations, and purified using the UltraClean PCR Clean-Up Kit (Qiagen, Carlsbad, USA). Sequencing was conducted on the Illumina HiSeq 2500 platform (San Diego, USA) to generate 250 bp paired-end reads.

Raw sequence quality was evaluated using FastQC, and low-quality reads were filtered with Sickle, retaining only those with a minimum Phred quality score of 20. Paired-end reads were merged into single sequences using the QIIME v1.8 pipeline, and sequences containing homopolymer runs, ambiguous bases, primer mismatches, barcode errors, or lengths <300 bp were removed. Quality-filtered sequences were demultiplexed based on unique barcode identifiers[2]. Operational taxonomic units (OTUs) were assigned using the Ribosomal Database Project (RDP) Classifier[5] against the Greengenes database (v13.8)[6] for bacteria and the UNITE database (release its_12_11_otus)[7] for fungi. OTU tables were rarefied to a sequencing depth of 4,800 reads per sample for bacteria and 2,400 reads per sample for fungi to standardize sampling effort. Microbial alpha diversity was assessed using the Shannon diversity index, calculated with the 'vegan' package in R.

Supplementary Figures

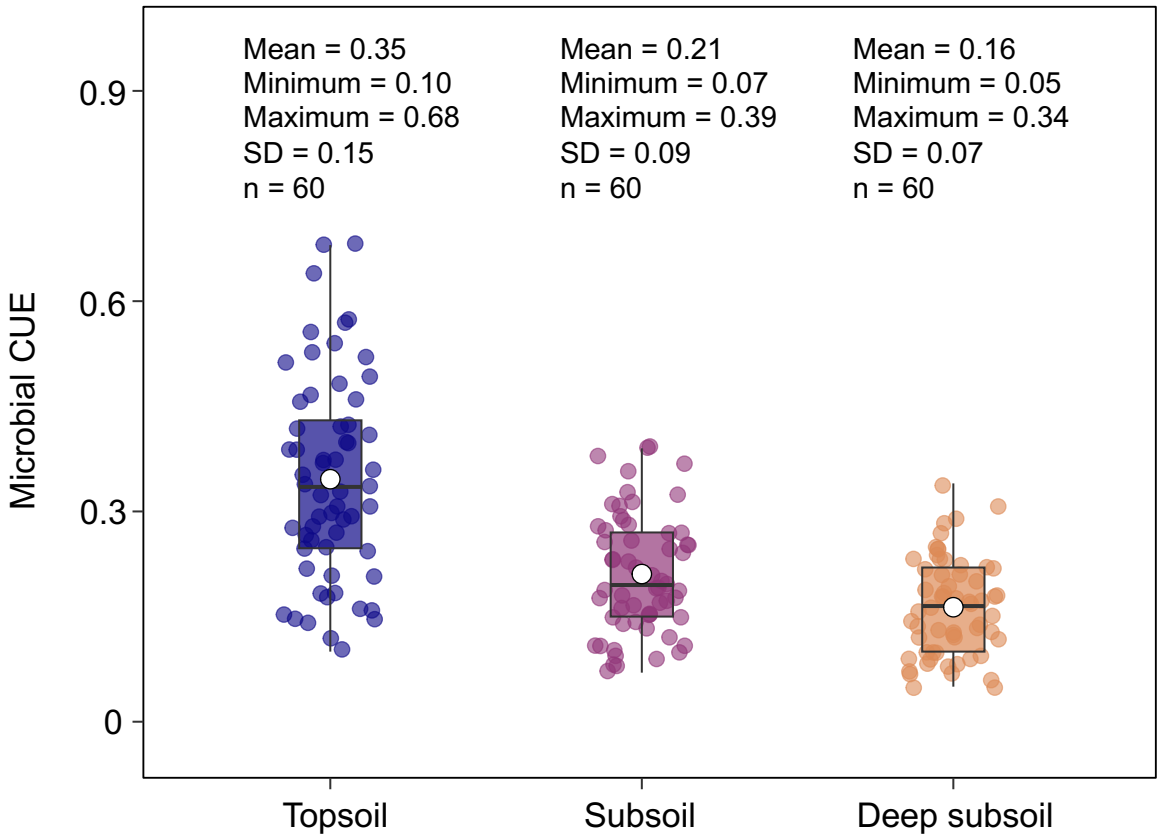

Supplementary Fig. 1 | Variability in microbial carbon use efficiency (CUE) at different soil horizons. Box edges represent the first and third quartiles, whiskers extend within the interquartile range, and horizontal lines inside the boxes indicate the median. White dots denote mean values, while colored dots represent individual data points.

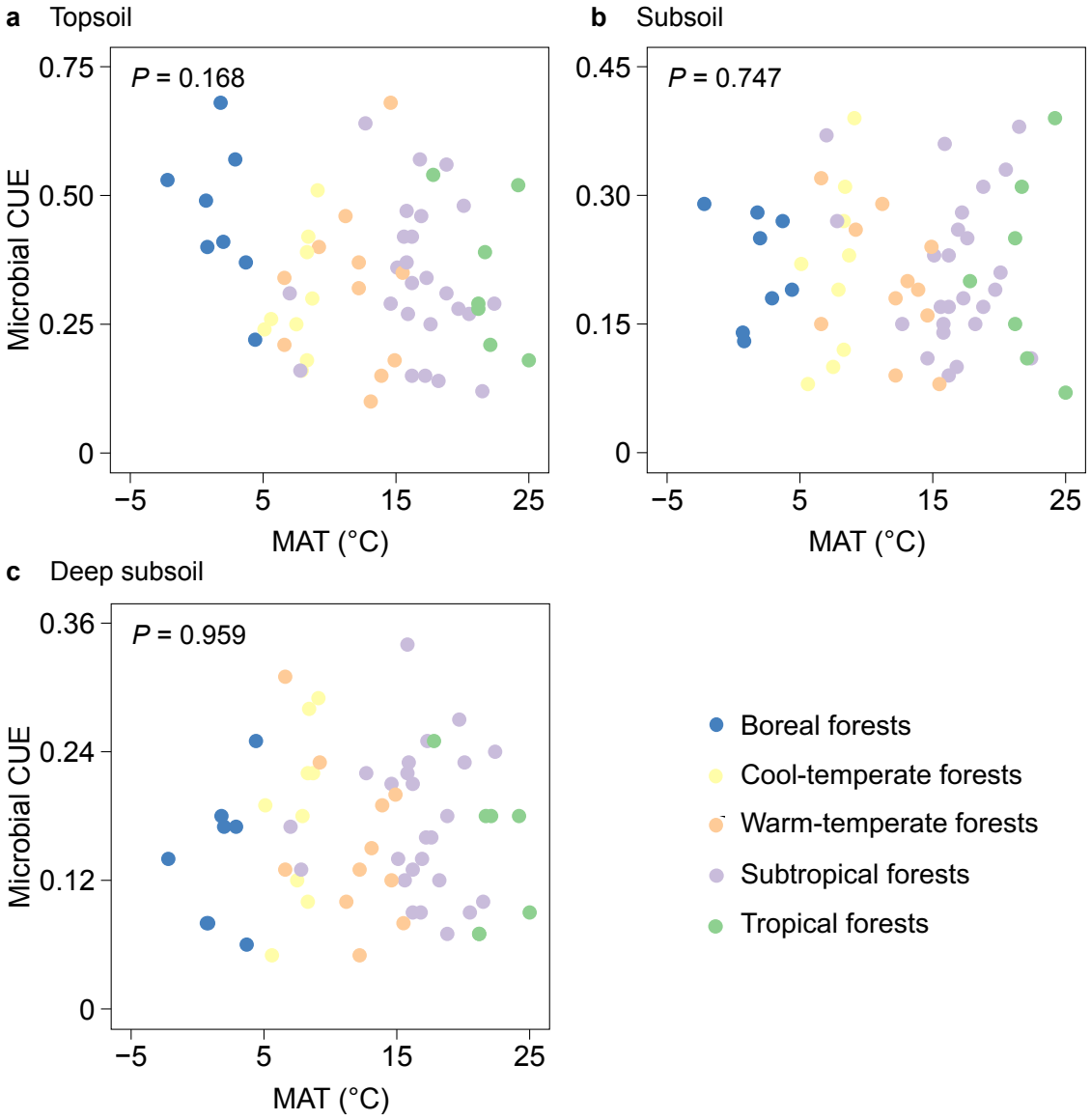

Supplementary Fig. 2 | Relationships between microbial CUE and MAT. a–c, Linear regressions depicting the relationship between CUE and MAT in the topsoil (0–10 cm, **a**), subsoil (35–50 cm, **b**) and deep subsoil (70–100 cm, **c**). The dots correspond to individual values (n = 32, 50 and 47 for topsoil, subsoil and deep subsoil, respectively). CUE, carbon use efficiency; MAT, mean annual temperature.

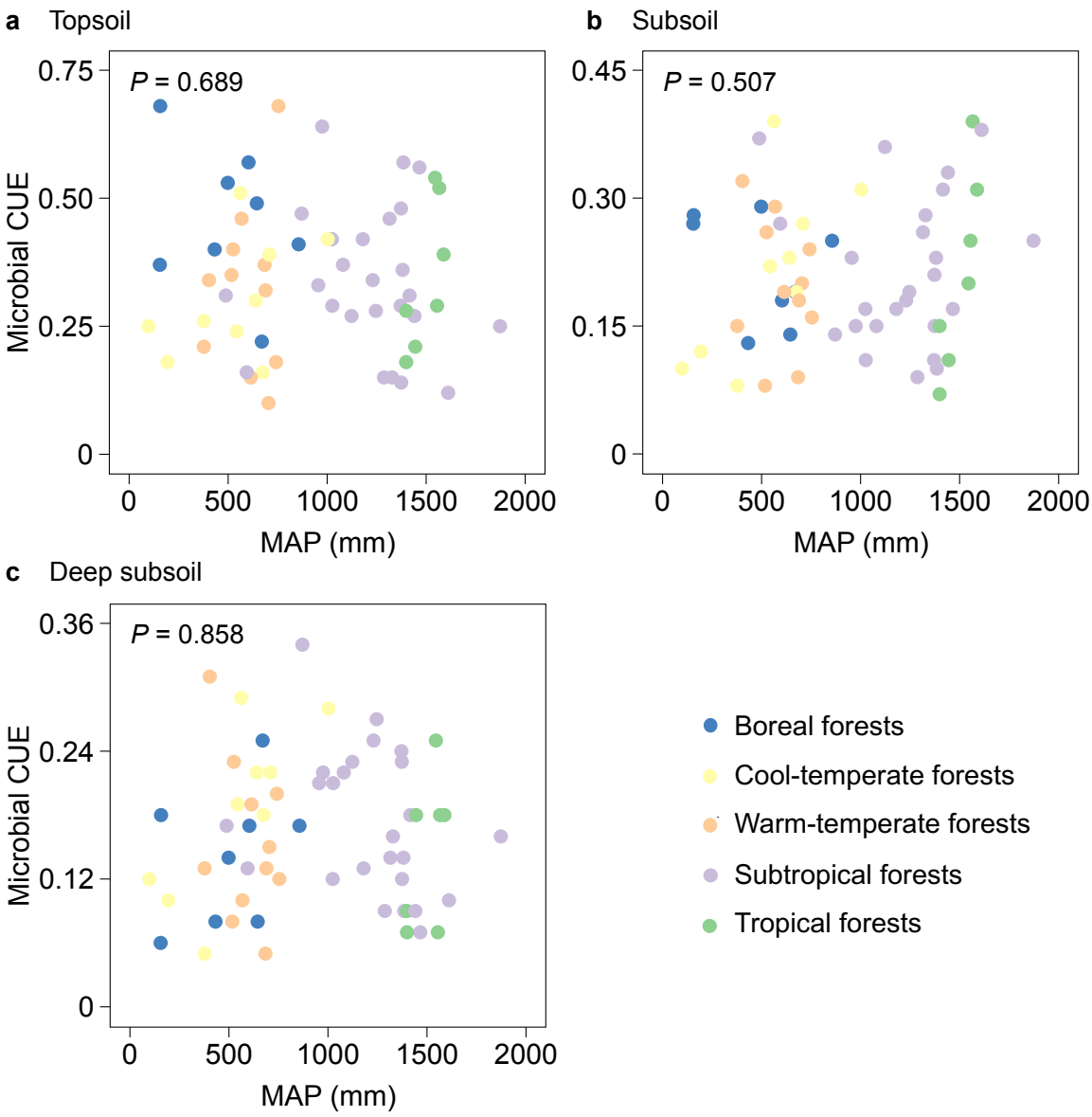

Supplementary Fig. 3 | Relationships between microbial CUE and MAP. a–c, Linear regressions depicting the relationship between CUE and MAP in the topsoil (0–10 cm, **a**), subsoil (35–50 cm, **b**) and deep subsoil (70–100 cm, **c**). The dots correspond to individual values (n = 32, 50 and 47 for topsoil, subsoil and deep subsoil, respectively). CUE, carbon use efficiency; MAT, mean annual precipitation.

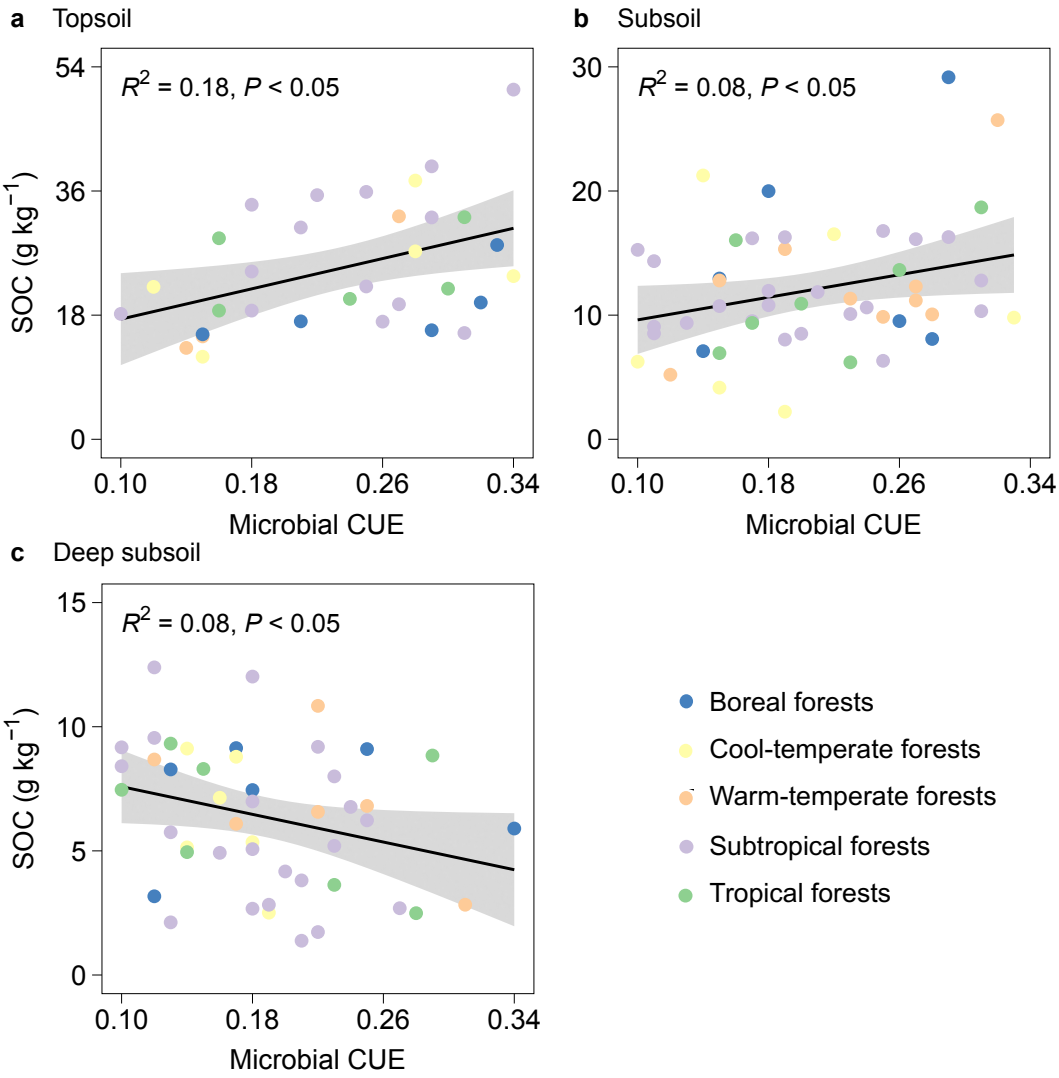

Supplementary Fig. 4 | Depth-dependent relationships between SOC and microbial CUE with standardized CUE values across all soil horizons. a–c, Linear regressions depicting the relationship between SOC and standardized CUE values in the topsoil (0–10 cm, **a**), subsoil (35–50 cm, **b**) and deep subsoil (70–100 cm, **c**). The dots correspond to individual values (n = 32, 50 and 47 for topsoil, subsoil and deep subsoil, respectively). The solid lines are the linear regression lines, while the shaded grey areas represent the 95% confidence intervals. Note that CUE values have been standardized to the same range across all soil horizons for consistency. CUE, carbon use efficiency; SOC, soil organic carbon.

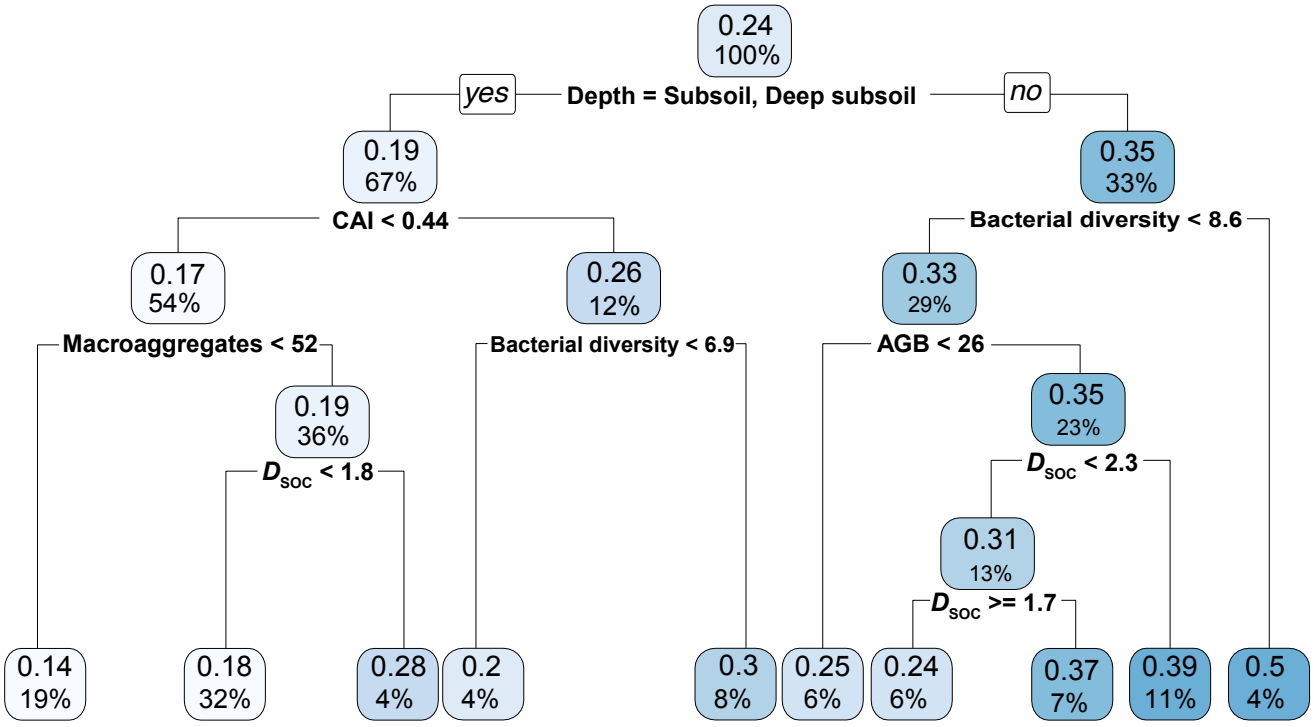

Supplementary Fig. 5 | Classification and regression tree illustrating how predictor variables explain microbial carbon use efficiency (CUE) across all soil horizons. Each panel displays the mean value of microbial CUE along with the percentage of sample size. The predictor variables are split at their respective thresholds in each branch, with the left and right sides of each branch representing values less than, equal to, or greater than the corresponding threshold. AGB, aboveground biomass carbon; CAI, carbon availability index; DSOC, decomposability of SOC.

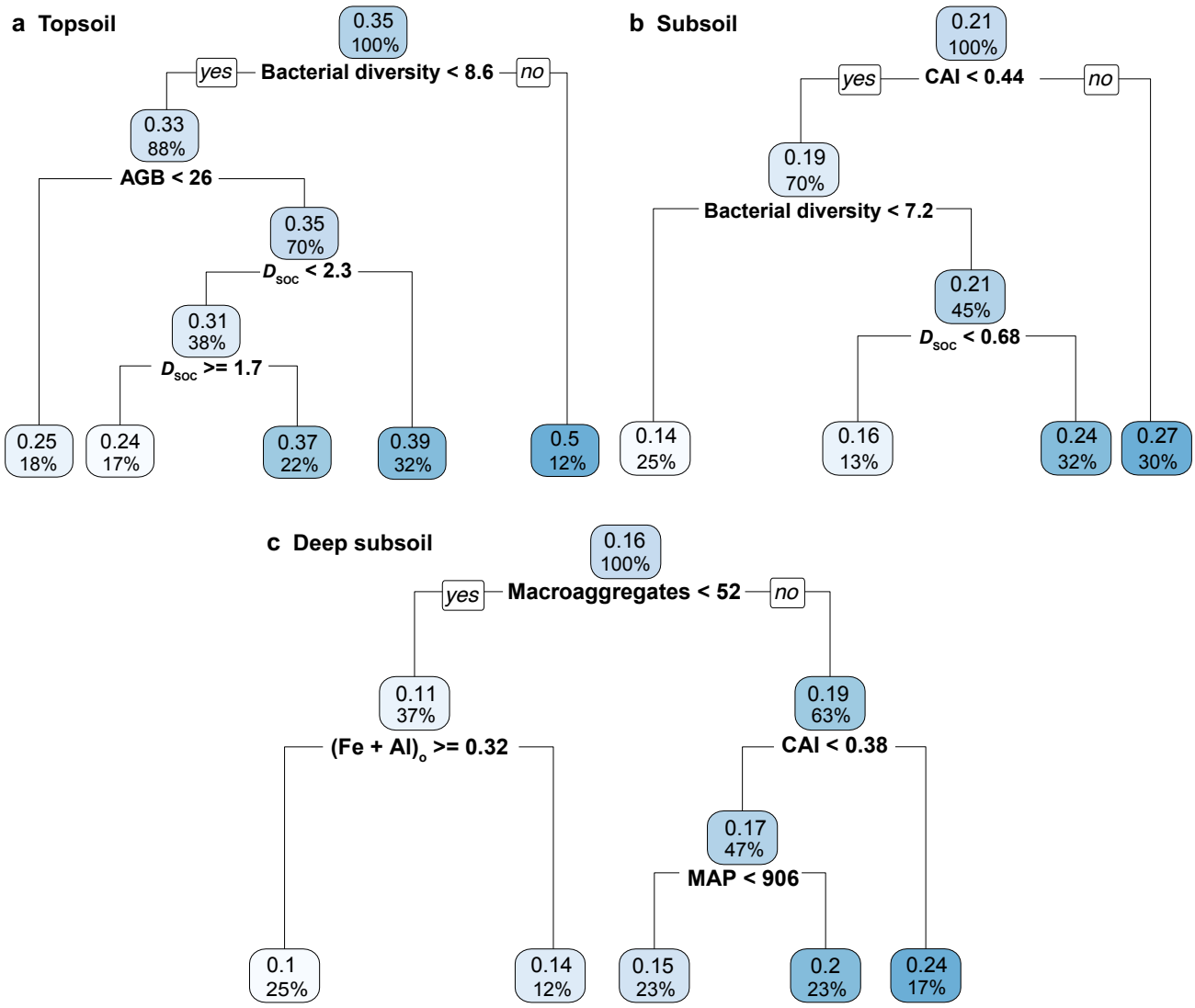

Supplementary Fig. 6 | Classification and regression tree showing how predictor variables explain microbial carbon use efficiency (CUE) for the topsoil (a), subsoil (b), and deep subsoil (c). Each panel displays the mean value of microbial CUE along with the percentage of sample size. The predictor variables are split at their respective thresholds in each branch, with the left and right sides of each branch representing values less than, equal to, or greater than the corresponding threshold. MAP, mean annual precipitation; AGB, aboveground biomass carbon; CAI, carbon availability index; D_{SOC}, decomposability of SOC.

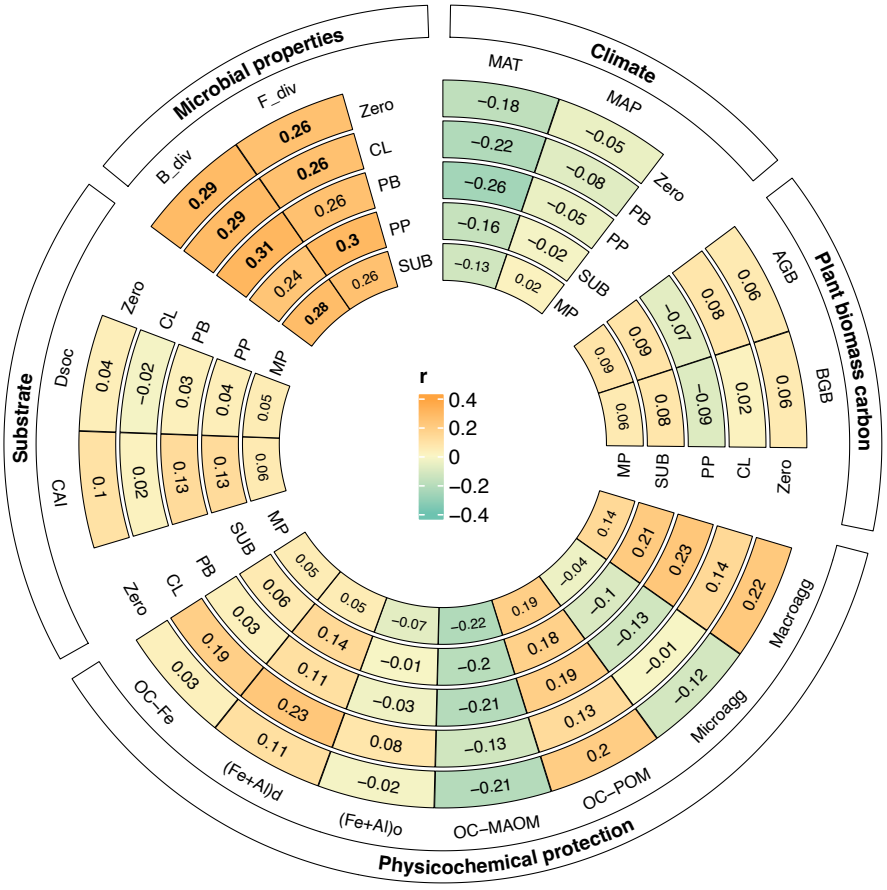

Supplementary Fig. 7 | Partial correlations of microbial carbon use efficiency (CUE) with climate, plant biomass carbon, physicochemical protection, substrate and microbial communities in the topsoil (0–10 cm). The outermost circles represent variables analyzed for their correlations with microbial CUE. The color of the fan segments indicates the strength and direction of the correlation, with bold numbers denoting statistically significant correlations at $P < 0.05$. Differences in color between the zero-order correlation (Zero) and controlled variables illustrate the dependency of the correlation on the controlled variable (e.g., a decrease or increase in color intensity suggests a loss or gain of correlation, while no color change indicates no dependency). CL, climate; PB, plant biomass carbon; PP, physicochemical protection; SUB, substrate; MP, microbial properties; MAT, mean annual temperature; MAP, mean annual precipitation; AGB, aboveground biomass carbon; BGB, belowground biomass carbon; OC-POM, content of SOC stored in the POM fraction; OC-MAOM, content of SOC stored in the MAOM fraction; OC-Fe, content of SOC associated with Fe oxides; Macroagg, SOC stored in macroaggregates; Microagg, SOC stored in microaggregates; CAI, carbon availability index; D_{SOC}, decomposability of SOC; B_div, bacterial diversity; F_div, fungal diversity.

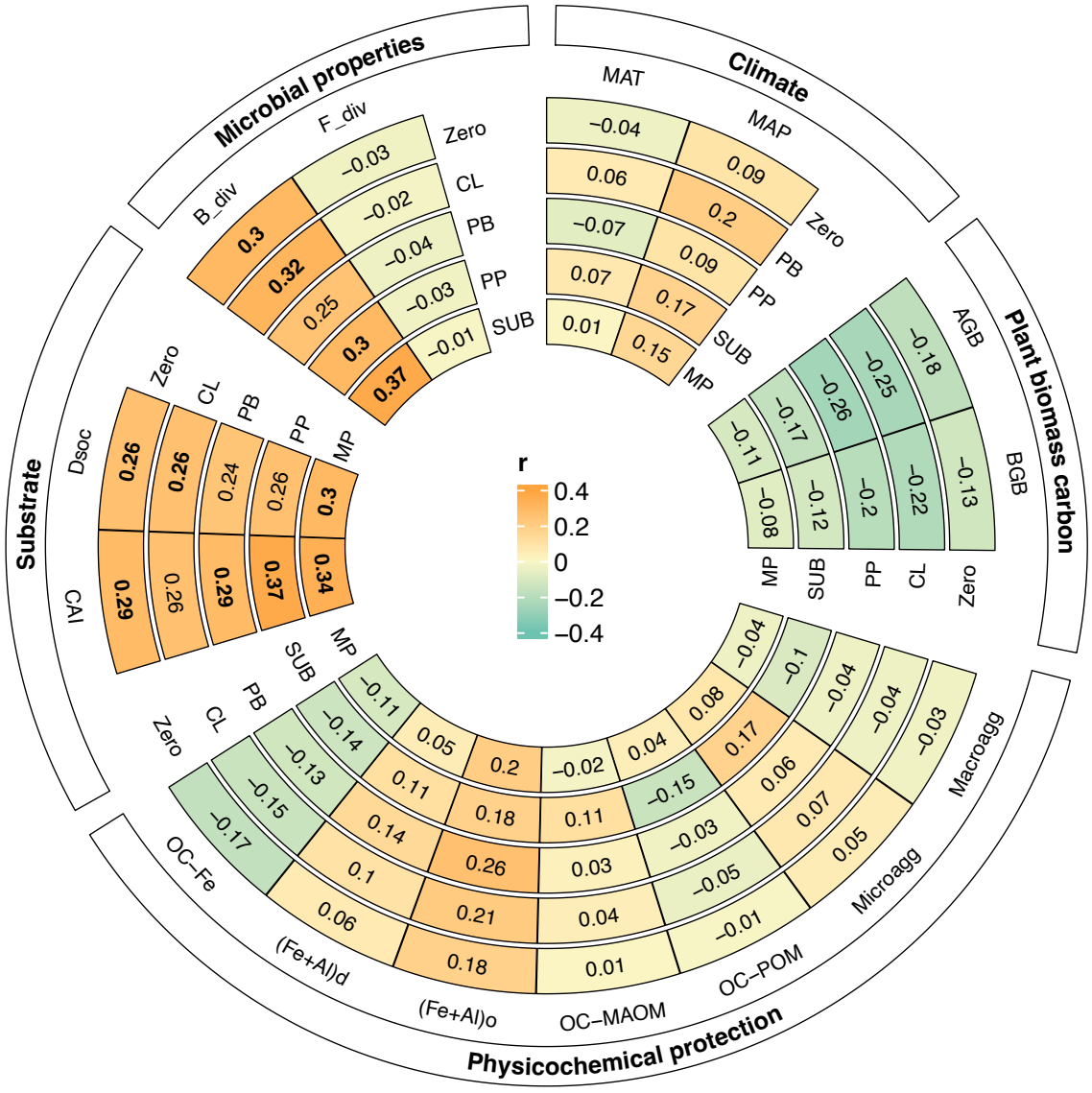

Supplementary Fig. 8 | Partial correlations of microbial carbon use efficiency (CUE) with climate, plant biomass carbon, physicochemical protection, substrate and microbial communities in the subsoil (35–50 cm). The outermost circles represent variables analyzed for their correlations with microbial CUE. The color of the fan segments indicates the strength and direction of the correlation, with bold numbers denoting statistically significant correlations at $P < 0.05$. Differences in color between the zero-order correlation (Zero) and controlled variables illustrate the dependency of the correlation on the controlled variable (e.g., a decrease or increase in color intensity suggests a loss or gain of correlation, while no color change indicates no dependency). All individual symbols are the same as those in Supplementary Fig. 7.

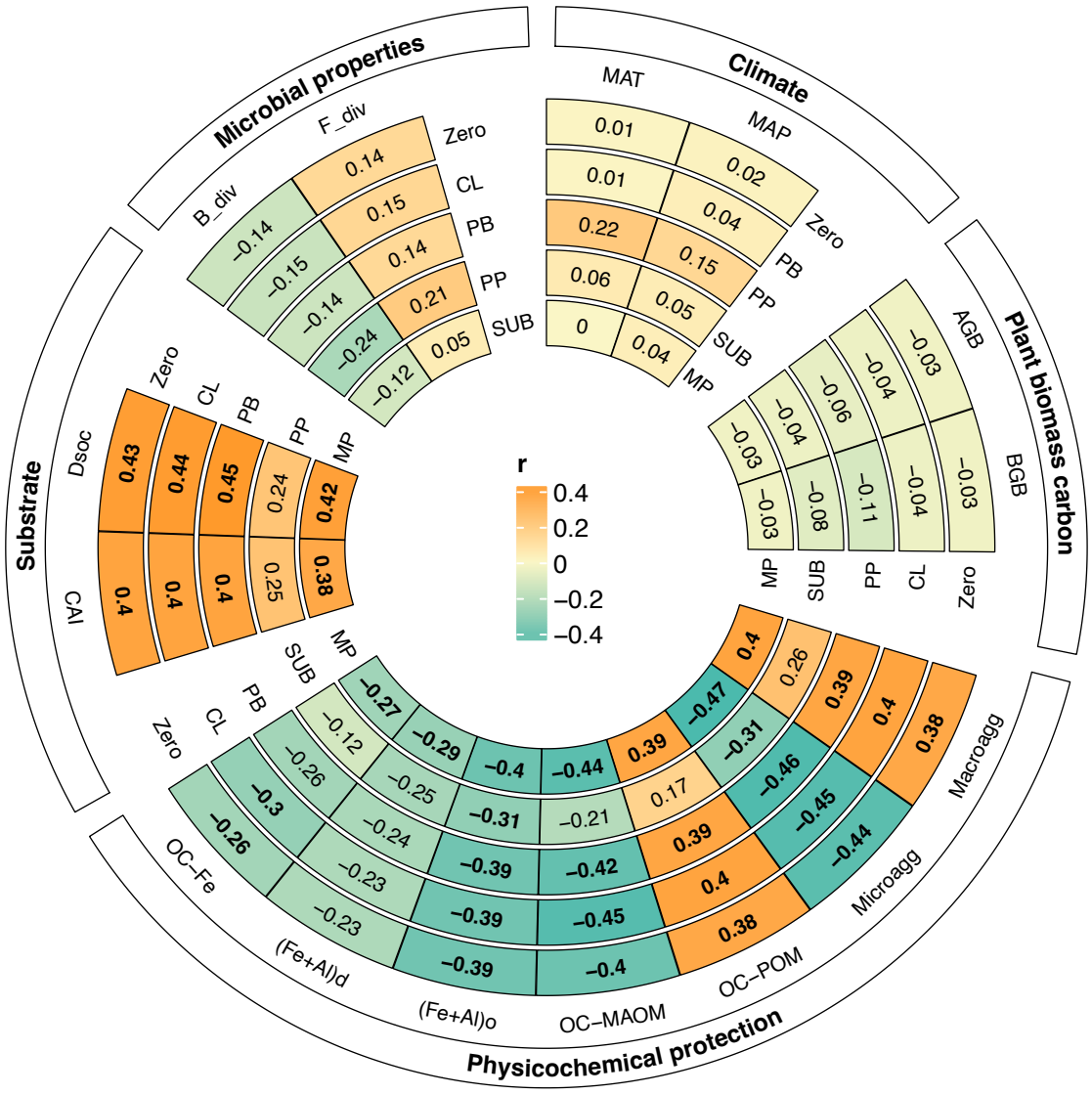

Supplementary Fig. 9 | Partial correlations of microbial carbon use efficiency (CUE) with climate, plant biomass carbon, physicochemical protection, substrate and microbial communities in the deep subsoil (70–100 cm). The outermost circles represent variables analyzed for their correlations with microbial CUE. The color of the fan segments indicates the strength and direction of the correlation, with bold numbers denoting statistically significant correlations at $P < 0.05$. Differences in color between the zero-order correlation (Zero) and controlled variables illustrate the dependency of the correlation on the controlled variable (e.g., a decrease or increase in color intensity suggests a loss or gain of correlation, while no color change indicates no dependency). All individual symbols are the same as those in Supplementary Fig. 7.

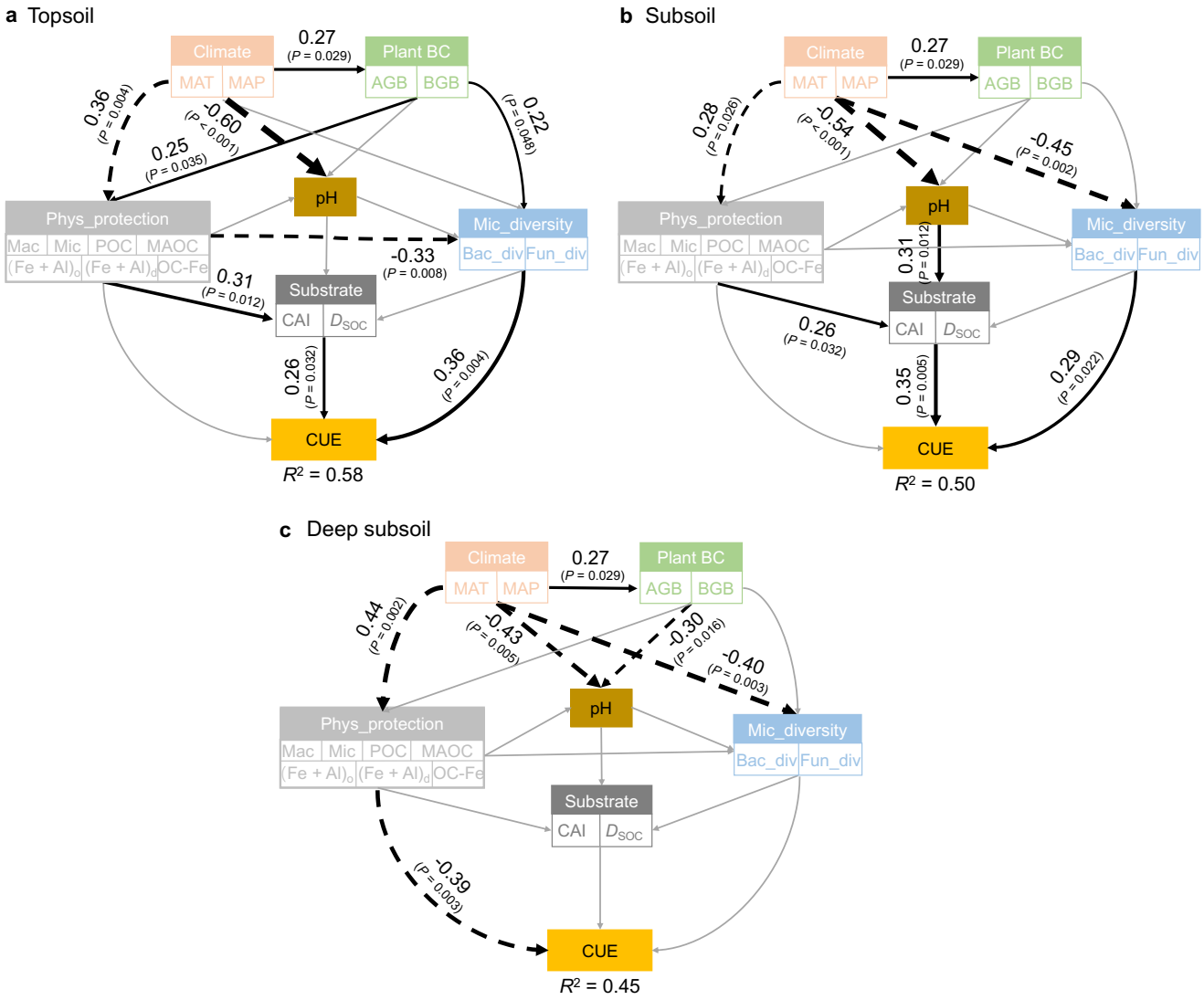

Supplementary Fig. 10 | Influencing pathways of biotic and abiotic factors on microbial carbon use efficiency (CUE) across soil horizons. a–c, Structural equation models illustrating the direct and indirect effects of various factor groups on CUE in the topsoil (**a**), subsoil (**b**) and deep subsoil (**c**). Pentagons represent the first principal component of the corresponding factor group, derived from principal component analysis, including climate, plant biomass, physicochemical protection, substrate and microbial properties. Black dashed and solid arrows indicate significant negative and positive relationships ($P < 0.05$), respectively, while gray arrows indicate nonsignificant relationships ($P > 0.05$). Numbers adjacent to the arrows represent standardized path coefficients with the exact P values. All individual symbols are the same as those in Supplementary Fig. 7.

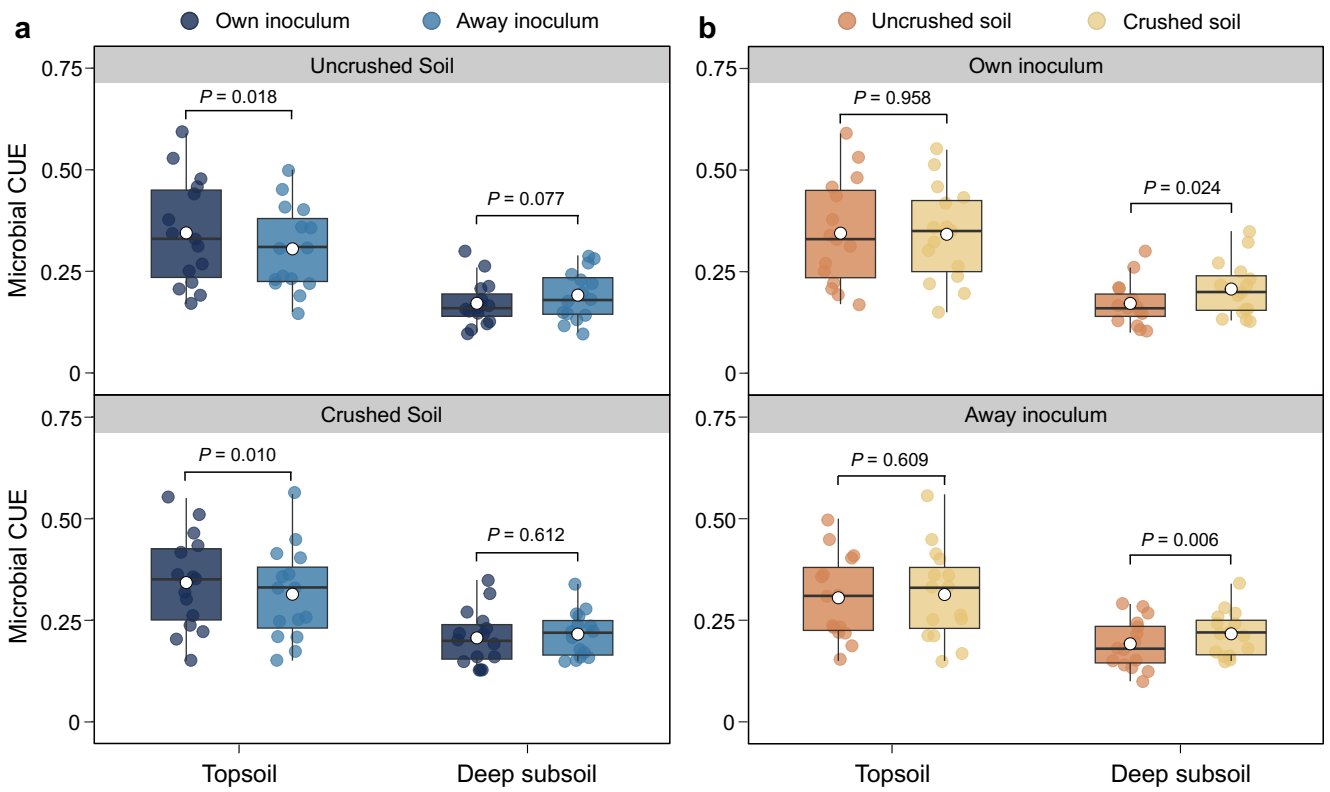

Supplementary Fig. 11 | Influence of microbial communities and aggregate protection on microbial carbon use efficiency (CUE) in topsoil and deep subsoil through microbial reciprocal transplantation and aggregate disruption. a, Differences in CUE between soils inoculated with native (own) and non-native (away) microbial communities. **b**, Differences in CUE between soils with and without aggregate protection removal. The ends of the boxes represent the first and third quartiles, whiskers extend to the interquartile range, and the horizontal lines within the boxes indicate the median. White dots within the boxes denote mean values, while colored dots represent individual data points (n = 15). Statistical analysis was performed using a two-sided, paired samples t-test.

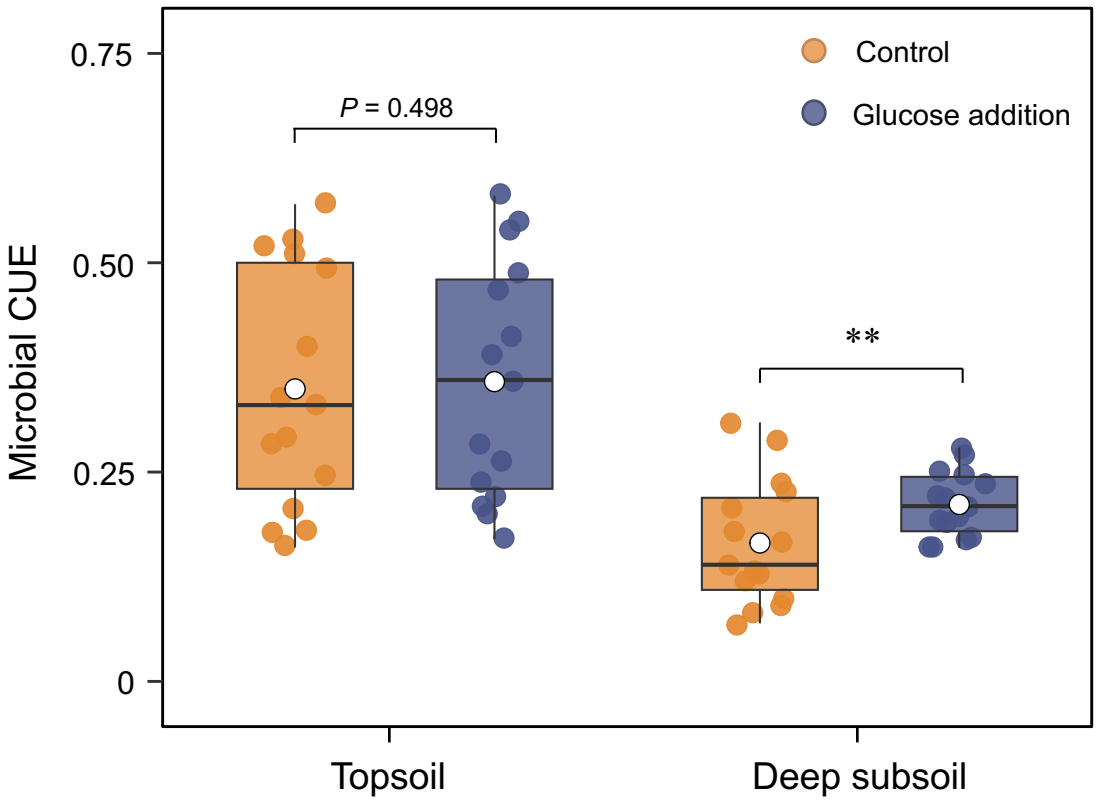

Supplementary Fig. 12 | Effects of glucose addition on microbial carbon use efficiency (CUE). The ends of the boxes represent the first and third quartiles, while the whiskers extend to the interquartile range from these quartiles. The horizontal line inside each box indicates the median. White dots within the box plots represent mean values, while colored dots correspond to individual data points ($n = 15$). $^{**}P < 0.01$, significant difference between control and treatment.

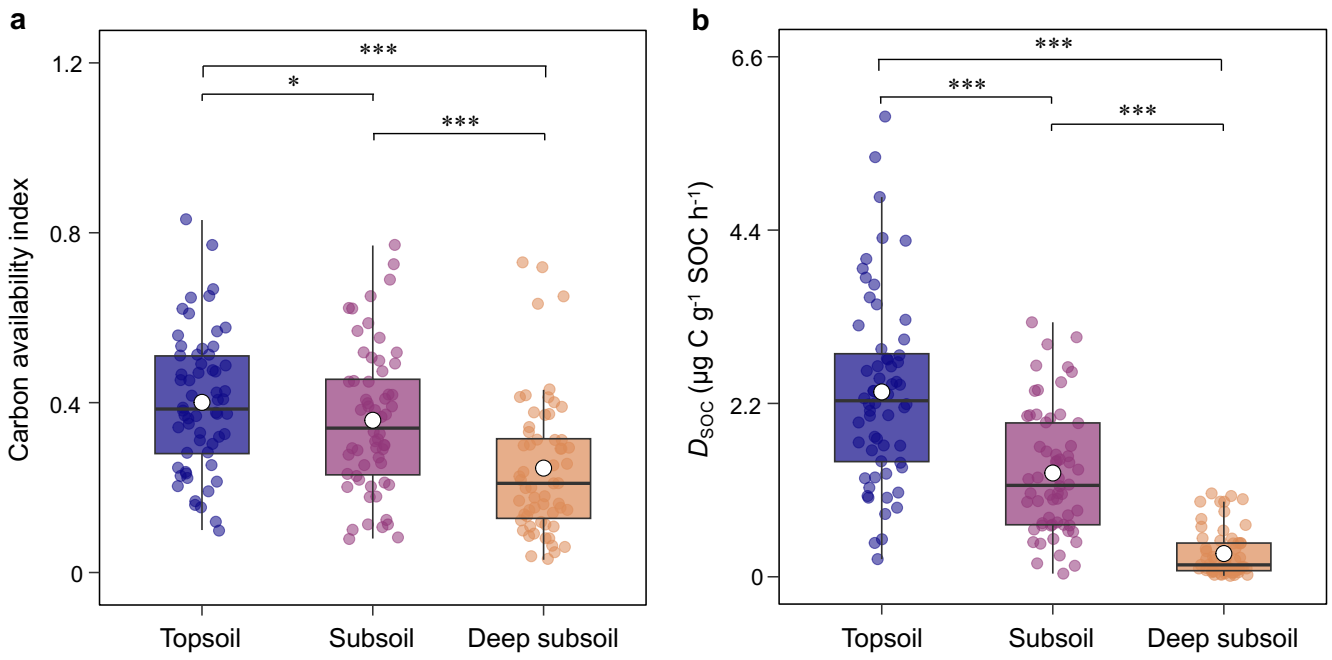

Supplementary Fig. 13 | Variations in substrate availability and quality across different soil horizons. a–b, Box plots illustrating carbon availability index (**a**) and carbon quality indicated by the decomposability of soil organic carbon (D_{SOC}; **b**) among soil horizons. The ends of the boxes represent the first and third quartiles, while the whiskers extend to the interquartile range from these quartiles. The horizontal lines inside the boxes indicate the median values. White dots within the box plots represent the mean values, and colored dots correspond to individual data points (n = 60). *P < 0.05, ***P < 0.001.

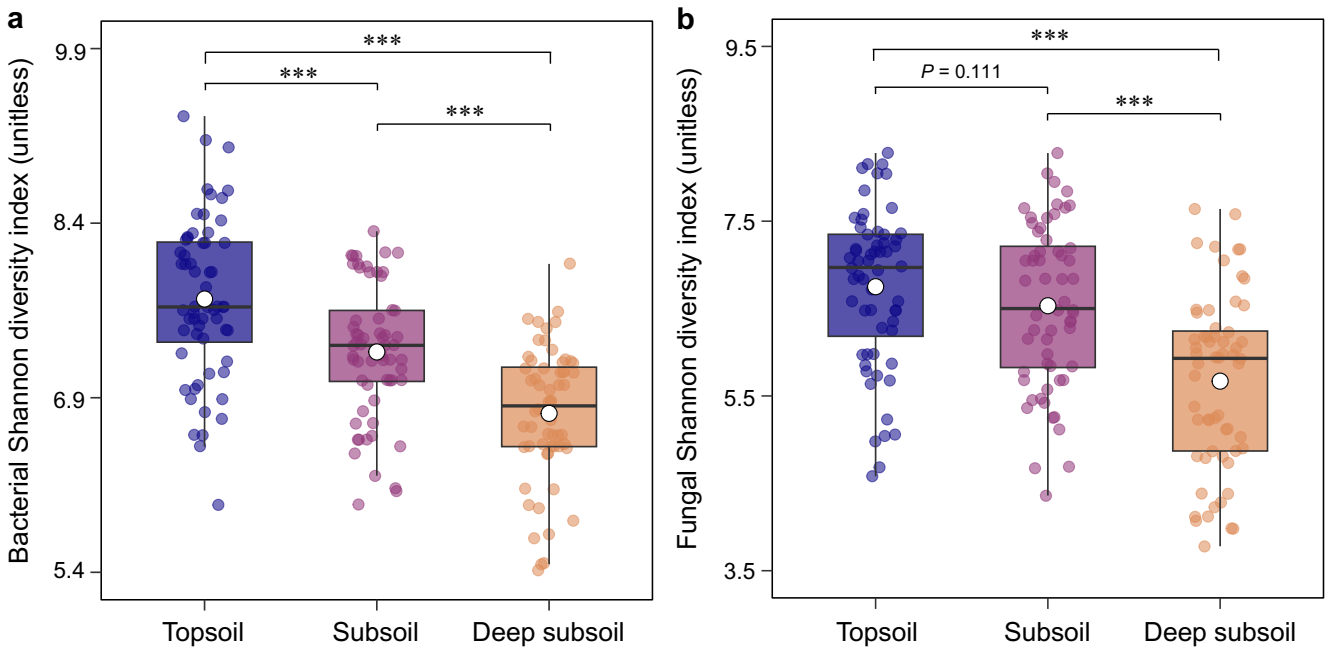

Supplementary Fig. 14 | Variations in bacterial and fungal diversity across different soil horizons. **a–b**, Box plots illustrating bacterial Shannon diversity index (**a**) and fungal Shannon diversity index (**b**) among soil horizons. The ends of the boxes represent the first and third quartiles, while the whiskers extend to the interquartile range from these quartiles. The horizontal lines inside the boxes indicate the median values. White dots within the box plots represent the mean values, and colored dots correspond to individual data points ($n = 60$). ***$P < 0.001$.

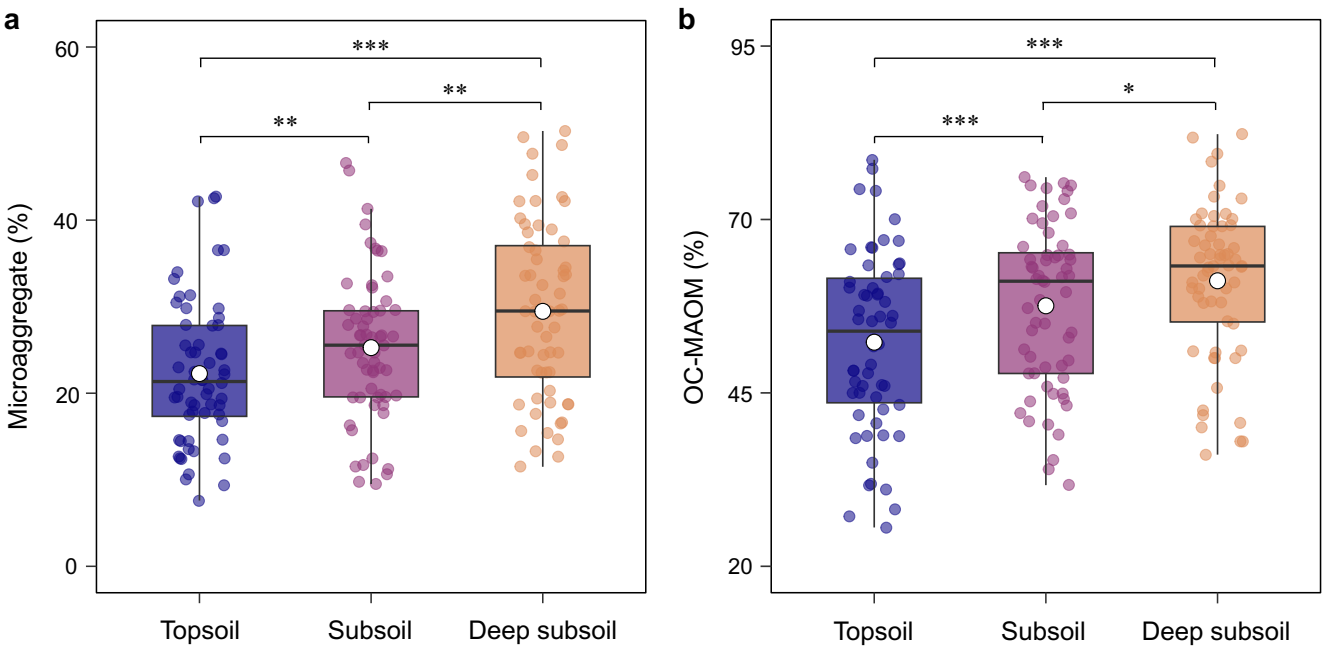

Supplementary Fig. 15 | Variations in physicochemical protection across different soil horizons. a–b, Box plots illustrating the soil organic carbon stored in microaggregate (**a**) and in mineral-associated organic matter (OC-MAOM; **b**) among soil horizons. The ends of the boxes represent the first and third quartiles, while the whiskers extend to the interquartile range from these quartiles. The horizontal lines inside the boxes indicate the median values. White dots within the box plots represent the mean values, and colored dots correspond to individual data points ($n = 60$). *$P < 0.05$, **$P < 0.01$, ***$P < 0.001$.

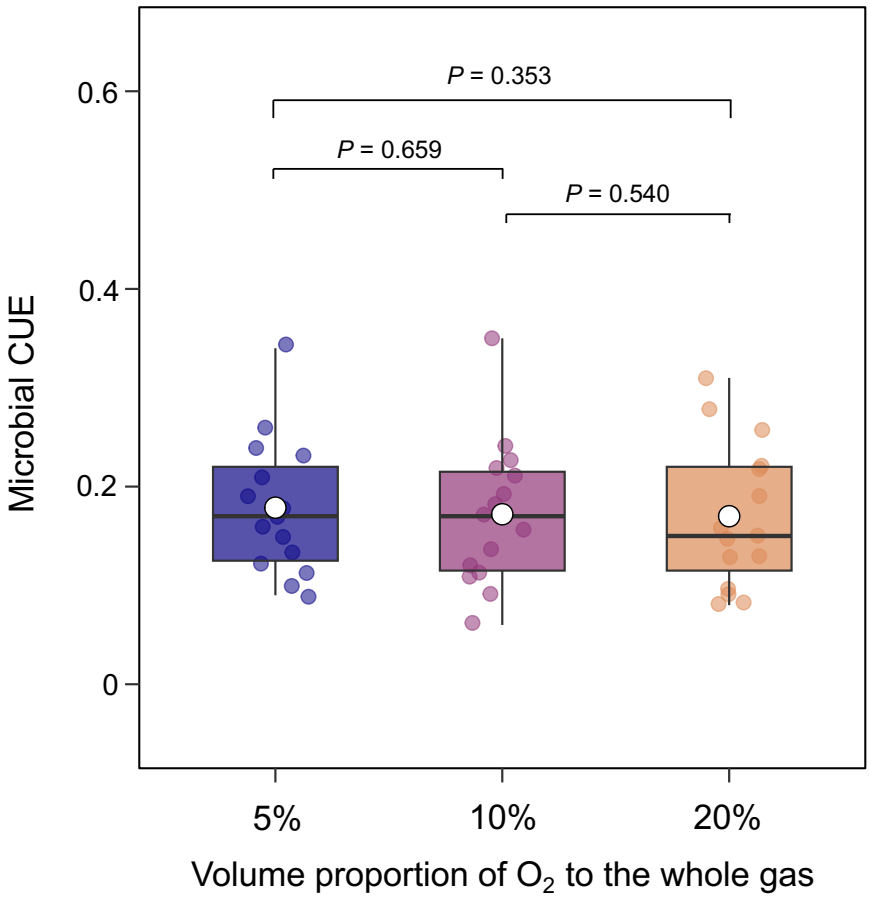

Supplementary Fig. 16 | Variations in microbial carbon use efficiency (CUE) under different oxygen levels. Oxygen levels are represented as 5%, 10%, and 20%, indicating the proportion of O_2 in a gas mixture composed of O_2 and N_2. For instance, a 5% oxygen level means the gas consists of 5% O_2 and 95% N_2. The ends of the boxes denote the first and third quartiles, with whiskers extending to the interquartile range. The horizontal lines inside the boxes indicate the median values. White dots within the box plots represent the mean values, while colored dots correspond to individual data points (n = 15).

Supplementary references

1. Tedersoo, L. et al. Global diversity and geography of soil fungi. *Science* **346**, 1256688 (2014).
2. Hamady, M., Walker, J. J., Harris, J. K., Gold, N. J. & Knight, R. Error-correcting barcoded primers for pyrosequencing hundreds of samples in multiplex. *Nat Methods* **5**, 235–237 (2008).
3. Apprill, A., McNally, S., Parsons, R. & Weber, L. Minor revision to V4 region SSU rRNA 806R gene primer greatly increases detection of SAR11 bacterioplankton. *Aquat Microb Ecol* **75**, 129–137 (2015).
4. Parada, A. E., Needham, D. M. & Fuhrman, J. A. Every base matters: assessing small subunit rRNA primers for marine microbiomes with mock communities, time series and global field samples. *Environ Microbiol* **18**, 1403–1414 (2016).
5. Wang, Q., Garrity, G. M., Tiedje, J. M. & Cole, J. R. Naïve Bayesian Classifier for Rapid Assignment of rRNA Sequences into the New Bacterial Taxonomy. *Appl. Environ. Microbiol.* **73**, 5261–5267 (2007).
6. McDonald, D. et al. An improved Greengenes taxonomy with explicit ranks for ecological and evolutionary analyses of bacteria and archaea. *ISME J.* **6**, 610–618 (2012).
7. Kõljalg, U. et al. Towards a unified paradigm for sequence-based identification of fungi. *Mol. Ecol.* **22**, 5271–5277 (2013).